Journal of Electronic Research and Application, 2026, Volume 10, Issue 2
http://ojs.bbwpublisher.com/index.php/JERA
ISSN Online: 2208-3510
ISSN Print: 2208-3502

Near-Room-Temperature Performance Characterization of InAsSb XBn Devices

Dongqiong Chen[1], Hairong Wang[1], Rujie Li[1], Gongrong Deng[2]

[1]Yunnan Open University, Kunming, Yunnan 650504, China
[2]Kunming Institute of Physics, Kunming, Yunnan 650225, China

Abstract: This research aims to enhance the operating temperature of mid-infrared InAsSb XBn detectors (~4.5 μm cutoff) through specific device architecture. Measurements performed under front-side illumination without an antireflection coating showed that at 290 K, the quantum efficiency was 34% for nBn devices compared to 45% for pBn devices. The nBn and pBn devices displayed distinct performance metrics at 290 K under a 500-mV reverse bias. The nBn devices recorded a dark current density of 0.348 A/cm^2 and a peak specific detectivity of 8.24×10^8 cm·Hz$^{1/2}$/W, whereas the pBn devices demonstrated improved characteristics with values of 0.536 A/cm^2 and 5.92×10^9 cm·Hz$^{1/2}$/W, respectively. The results indicate that these XBn structured barrier photodetectors exhibit excellent performance and demonstrate significant potential for near-room temperature applications.

Keywords: InAsSb; HOT; Photodetector; XBn

Online publication: March 4, 2026

1. Introduction

InAsSb is a highly competitive material for infrared detection, offering high spectral resolution, spatial resolution, and sensitivity due to its high carrier mobility, long minority carrier lifetime, tunable bandgap, strong absorption coefficient, and excellent stability [1,2]. Uncooled InAsSb infrared photodetectors are widely used in commercial, scientific, and defence applications owing to their compact size, low cost, and low power consumption. However, at elevated operating temperatures, a large number of intrinsic charge carriers are thermally excited, leading to increased dark current [3–5]. This rise in dark current, in turn, intensifies various types of noise, such as shot noise, 1/f noise, and excess noise, while the enhanced random thermal motion of carriers also contributes to higher thermal noise in the infrared detector.

In 2006, Professor Maimon and Wicks first introduced the nBn barrier structure, by incorporating a wide-bandgap barrier layer, this design eliminates the depletion region within the narrow bandgap semiconductor, thereby suppressing dark current and enabling higher operating temperatures for infrared detectors [6]. To date, barrier structures have achieved significant progress in bulk materials, type-II superlattices, and two-dimensional

materials [7–14].

In this study, we evaluated the near-room-temperature performances of MWIR XBn InAsSb devices and demonstrated their potential for ambient-temperature operation. At room temperature, the detectors exhibited a 50% cut-off wavelength of approximately 4.5 μm. When characterized under a 500 mV reverse bias, the nBn detector yielded a dark current density of 0.348 A/cm^2 and a corresponding peak detectivity of 8.24×10^8 cm·Hz$^{1/2}$/W, while the pBn structure showed a dark current density of 0.536 A/cm^2, which corresponded to a higher peak specific detectivity of 5.92×10^9 cm·Hz$^{1/2}$/W. These findings enhance the understanding of high-temperature behavior in XBn detectors and will support further performance improvements in such devices.

2. Methodology

The $InAs_{0.91}Sb_{0.09}$-based XBn materials for this investigation were fabricated using a molecular beam epitaxy (MBE) system. The nBn detector structure was grown with the following layers in sequence: a GaSb substrate, a 200 nm GaSb buffer layer, a 500 nm n-doped $InAs_{0.91}Sb_{0.09}$ bottom contact layer (doping concentration: 1×10^{18}cm^{-3}), a 3000 nm unintentionally doped $InAs_{0.91}Sb_{0.09}$ absorption layer, a 150 nm unintentionally doped $AlAs_{0.08}Sb_{0.92}$/AlSb (1.5 nm/1.5 nm) digital alloy barrier layer, a 200 nm unintentionally doped $InAs_{0.91}Sb_{0.09}$ layer, and a 100 nm n-doped $InAs_{0.91}Sb_{0.09}$ top contact layer (doping concentration: 1×10^{17}cm^{-3}). In comparison, the pBn epitaxial structure, listed from top to bottom, includes: a 250 nm p-type GaSb top contact layer (doping concentration: 1.5×10^{17}cm^{-3}), a 150 nm AlAs/AlSb (1 ML/10 MLs) barrier layer, a 3000 nm unintentionally doped $InAs_{0.91}Sb_{0.09}$ absorption layer, and a 300 nm n-type $InAs_{0.91}Sb_{0.09}$ bottom contact layer (doping concentration: 5×10^{17}cm^{-3}). The n-type and p-type dopings were achieved using silicon (Si) and beryllium (Be), respectively.

Figure 1 presents the XRD patterns of the $InAs_{0.91}Sb_{0.09}$ nBn and pBn structural materials. All epitaxial layers, including the GaSb substrate, $InAs_{0.91}Sb_{0.09}$ absorption layer, and barrier layer, are clearly resolved. The diffraction peak of the $InAs_{0.91}Sb_{0.09}$ layer overlaps with that of the GaSb substrate, indicating an excel-lent lattice match between the absorption layer and the substrate. The narrow full width at half maximum (FWHM) of less than 20 arcsec attests to the high crystalline quality of the epitaxial $InAs_{0.91}Sb_{0.09}$ layers.

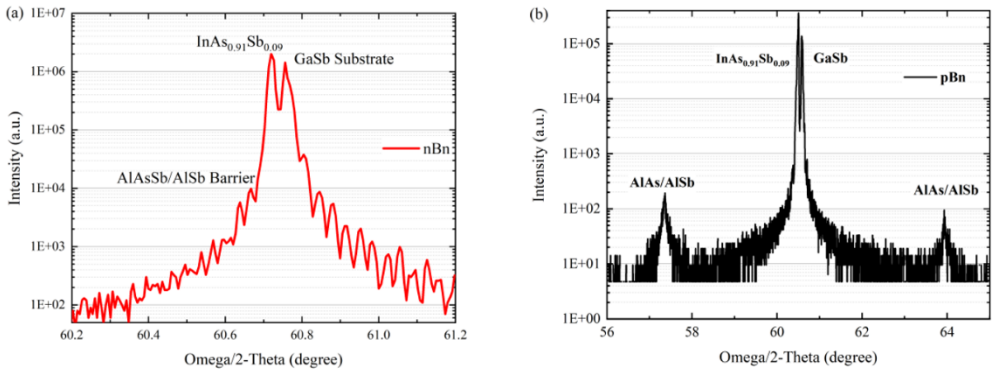

Figure 1. XRD patterns of the (a) nBn and (b) pBn epitaxial structures.

The energy band structures of $InAs_{0.91}Sb_{0.09}$ nBn and pBn devices were simulated using Sentaurus TCAD. As shown in **Figure 2**, under zero bias at 290 K, the offset of the valance band between the $InAs_{0.91}Sb_{0.09}$ absorption layer and the composite barrier is only 30 meV for the nBn device and 120 meV for the pBn device, posing a negligible barrier to minority holes. In contrast, the conduction band offset reaches approximately 1.377 eV,

effectively blocking majority electrons and thus suppressing both bulk and surface leakage currents.

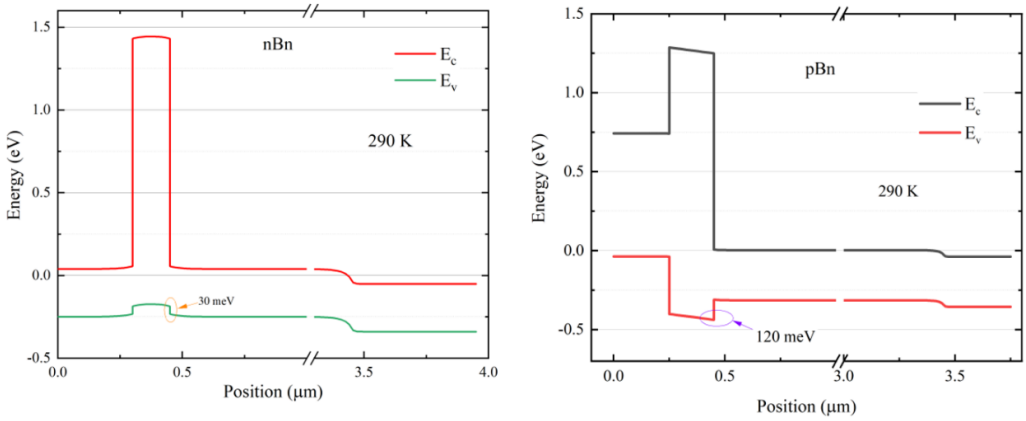

Figure 2. Band alignment of the (a) nBn and (b) pBn InAsSb devices.

The developed epitaxial materials were processed into circular single-element photodetectors with a diameter of 210 μm. Standard photolithography was employed to pattern the device structures, which were subsequently etched down to the $InAs_{0.91}Sb_{0.09}$ bottom contact layer using a hybrid dry-wet etching approach. The dry etching process introduced surface defects, which were effectively eliminated through 60-second wet etching in a citric acid-based solution. For mesa passivation, a 400 nm thick SiO_2 layer was deposited by inductively coupled plasma chemical vapor deposition (ICPCVD). Contact windows were then opened to both top and bottom contact layers using reactive ion etching (RIE), followed by electron-beam evaporation of 50/400 nm Cr/Au stacks to form ohmic contacts. The electrode patterning was finally completed through a standard acetone lift-off process.

3. Results and discussion

After fabrication, the dark current-voltage characteristics of the devices were tested using an Agilent B1500 analyzer. The devices were housed in a dewar featuring a cold shield for optical measurements. Under front-side lighting without the presence of any antireflection coating, the photodetectors' optical performances were evaluated. The responsivity and quantum efficiency were determined by using a calibrated 500℃ blackbody source. In the meantime, the relative spectral response were measured with the employment of a Fourier transform infrared (FTIR) spectrometer.

Figure 3(a) depicts the dark current characteristics of the InAsSb nBn device at near room-temperature. At a -500-mV bias voltage, the dark current densities of the device corresponding to 210 K, 230 K, 250 K, 270 K, and 290 K are 1.61×10^{-3} A/cm^2, 8.7×10-3 A/cm^2, 0.0418 A/cm^2, 0.156 A/cm^2, and 0.348 A/cm^2, respectively. **Figure 3(b)** shows the dark current characteristics of the InAsSb pBn device at near room-temperature. At a bias voltage of -400 mV, the dark current densities of the device at 210 K, 230 K, 250 K, 270 K, and 290 K are 2.27×10^{-3} A/cm^2, 8.57×10^{-3} A/cm^2, 0.0319 A/cm^2, 0.096 A/cm^2, and 0.536 A/cm^2, respectively. At near-room-temperature, the activation energies of the nBn and pBn devices, calculated from the Arrhenius plot, are both 305 meV, indicating that the dark currents of the devices are mainly governed by diffusion current in this regime.

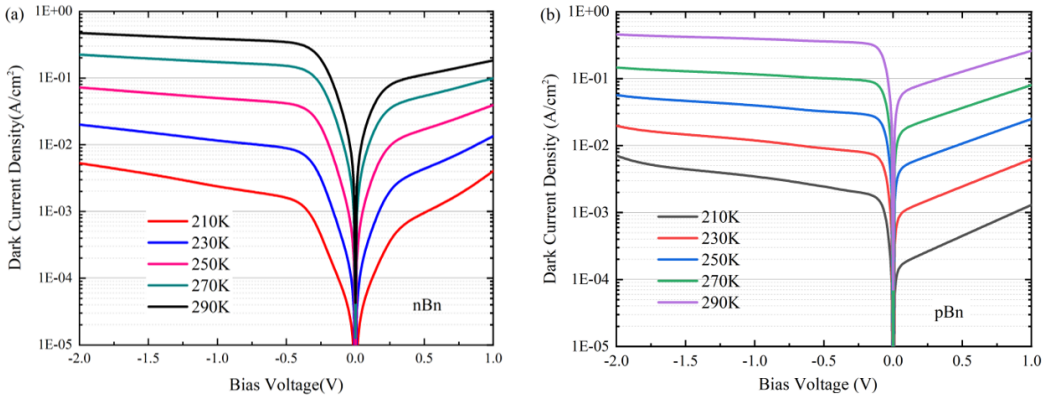

Figure 3. J-V characteristics of the (a) nBn and (b) pBn devices.

Figure 4 depicts the relative spectral response spectra for the processed mid-wave infrared (MWIR) photodetectors at near-room-temperature. The dip observed at 4.2 μm corresponds to CO2 absorption in the air. As can be seen from **Figure 4(a)**, as the operating temperature increases, the cutoff wavelength of the $InAs_{0.91}Sb_{0.09}$ nBn device exhibits a red shift. At operating temperatures of 210 K, 230 K, 250 K, 270 K, and 290 K, the cutoff wavelengths of the device are 4.27 μm, 4.29 μm, 4.32 μm, 4.48 μm, and 4.55 μm, respectively. **Figure 4(b)** presents the calculated quantum efficiency curve of the device. Since the device is front-illuminated, the top $InAs_{0.91}Sb_{0.09}$ layer absorbs a portion of the infrared light, resulting in a lower quantum efficiency compared to pBn devices. As the operating temperature increases, the quantum efficiency of the $InAs_{0.91}Sb_{0.09}$-nBn device decreases from 40% at 210 K to 34% at 290 K. The corresponding peak detectivities of the device are 2.47×10^{10} cm·Hz$^{1/2}$/W, 9.59×10^{9} cm·Hz$^{1/2}$/W, 4.0×10^{9}cm·Hz$^{1/2}$/W, 1.92×10^{9}cm·Hz$^{1/2}$/W and 8.24×10^{8} cm·Hz$^{1/2}$/W, respectively.

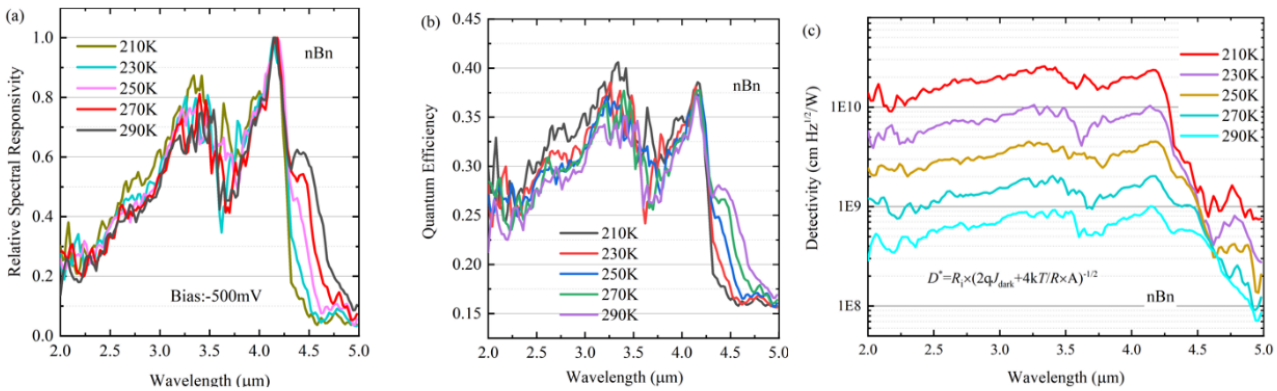

Figure 4. Measured performance spectra of the nBn photodetector at -500 mV reverse bias for (a) relative spectral responsivity, (b) saturated quantum efficiency, and (c) calculated saturated spe-cific detectivity.

Figure 5 characterizes the performances of the $InAs_{0.91}Sb_{0.09}$-pBn device across operating temperatures, showing the relative spectral response **(a)**, quantum efficiency **(b)**, and detectivity **(c)**. The cutoff wavelength exhibits a red shift from 4.23 μm to 4.5 μm as temperature increases from 210 K to 290 K, with specific measurements recorded at 4.23 μm, 4.29 μm, 4.33 μm, 4.37 μm, and 4.5 μm. The quantum efficiency is about 53% at 210 K and drops slightly to approximately 45% at 290 K. The corresponding peak detectivities are

9.22×10^{10} cm·Hz$^{1/2}$/W, 4.51×10^{10} cm·Hz$^{1/2}$/W, 2.29×10^{10} cm·Hz$^{1/2}$/W, 1.16×10^{10} cm·Hz$^{1/2}$/W, and 5.92×10^{9} cm·Hz$^{1/2}$/W.

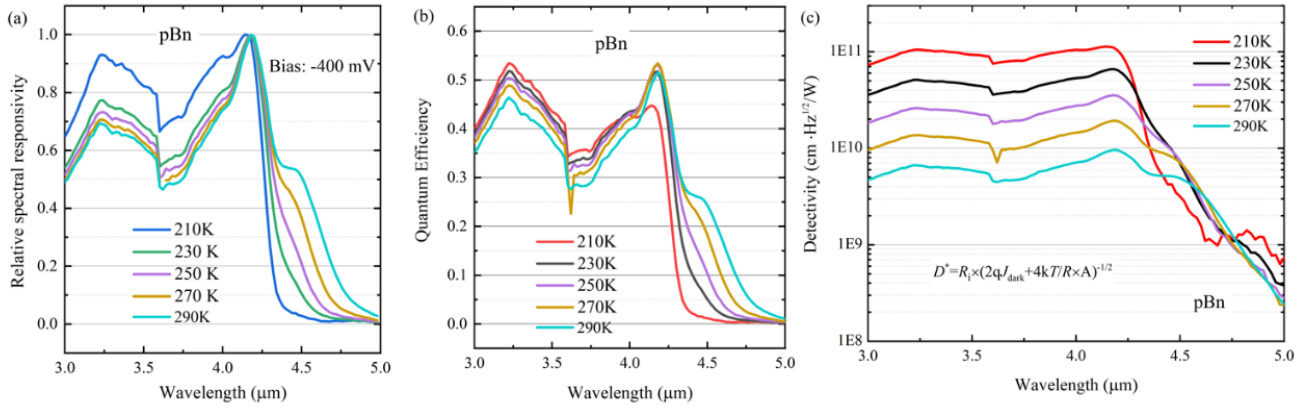

Figure 5. Measured performance spectra of the pBn photodetector at -400 mV reverse bias for (a) relative spectral responsivity, (b) saturated quantum efficiency, and (c) calculated saturated specific detectivity.

4. Conclusion

To summarize, we have successfully fabricated $InAs_{0.91}Sb_{0.09}$ XBn mid-wavelength infrared photodetectors and characterized their performances under near-room-temperature conditions. The devices exhibit the following characteristics: a 50% cutoff wavelength of approximately 4.5 μm; remarkably low dark current densities at room temperature, measured at only 0.348 A/cm^2 for the nBn structure and 0.536 A/cm^2 for the pBn structure; peak quantum efficiencies of 34% (nBn) and 45% (pBn), respectively; and calculated peak specific detectivities of 8.24×10^{8} cm·Hz$^{1/2}$/W for the nBn device and 5.92×10^{9} cm·Hz$^{1/2}$/W for the pBn device. These outstanding results demonstrate the significant potential of this XBn barrier photo-detector for near-room-temperature applications.

Funding

Scientific Research Foundation of Yunnan Provincial Department of Education (Project No.: 2024J0749)

Disclosure statement

The author declares no conflict of interest.

References

[1] Belenky G, Donetsky D, Kipshidze G, et al., 2011, Properties of Unrelaxed InAs1-xSbx Alloys Grown on Compositionally Graded Buffers. Appl. Phys. Lett., 2011(9): 141116.

[2] Rogalski A, Jó´zwikowski K, 1989, Intrinsic Carrier Concentration and Effec-tive Masses in InAs1−xSbx. Infrared Phys., 1989(29): 35–42.

[3] Deng G, Chen D, Yang S, 2020, High Operating Temperature pBn Barrier Mid-Wavelength Infrared Photodetectors and Focal Plane Array Based on InAs/InAsSb Strained Layer Superlattices. Opt. Express, 28(12): 17611.

[4] Xie H, 2023, Room-Temperature InAsSb pBin Detectors for Mid-Infrared Application. Infrared Phys. Technol.,

128(104000): 2023.

[5] Liu B, Zhu L, Lu L, et al., 2025, Fabrication and Dark Current Analysis of InAsSb-Based nBn Structures for High-Performance Mid-Infrared Applications. IEEE, 72(6): 3029–3034.

[6] Maimon S, Wicks G, 2006, nBn Detector, An Infrared Detector with Reduced Dark Current and Higher Operating Temperature. Appl. Phys. Lett., 89(15): 151109.

[7] Ting D, Soibel A, Khoshakhlagh A, et al., 2023, InAs/InAsSb Superlattice Infrared Detectors. Opto-Electron. Rev., 3122–45.

[8] Jang A, Lee H, Kim Y, 2022, Electrical Characteristics of a Ga-Free T2SL Mid-Wave Infrared nBn Detector Based on an InAs/AlAsSb/InAsSb Barrier. J. Electron. Mater., 2022(51): 4681–4688.

[9] She L, Jiang J, Chen W, 2022, Mid-Wave Infrared p+Bn InAs/InAsSb Type-II Superlattice Photodetector with an AlAsSb/InAsSb Superlattice Barrier. Infra-red Phys. Technol., 2022(121): 104015.

[10] Wu D, Li J, Dehzangi A, et al., 2020, Mid-Wavelength Infrared High Operating Temperature pBn Photodetectors Based on Type-II InAs/InAsSb Superlattice. AIP Adv., 2020(10): 025018.

[11] Xue T, Huang J, Zhang Y, et al., High Temperature Mid-Wave Infrared InAsSb Barrier Photodetectors. IEEE J. Quantum Electron., 60(2): 453–461.

[12] Lee H, Ko S, Kim Y, 2021, Surface Leakage Current Reduction of InAsSb nBn MWIR HOT Detector via Hydrogen Peroxide Treatment. Infrared Phys. Tech-nol., 2021(112): 103000.

[13] Huang S, Yan T, Xue Y, et al., 2022, Mid-Wavelength InAs/InAsSb Superlattice Photodetector with Background Limited Performance Temperature Higher than 160 K. IEEE Trans. Electron Devices, 69(8): 4392–4395.

[14] Linda H, Ting D, Soibel A, et al., 2025, Minority Carrier Lifetimes in InSb/InAsSb Quantum Dot and InAsSb nBn Photodetectors. IEEE, 27(23): 2492–2495.